Dynamical mean-field theory from a quantum chemical perspective

Dominika Zgid and Garnet Kin-Lic Chan

Citation: The Journal of Chemical Physics **134**, 094115 (2011); doi: 10.1063/1.3556707
View online: http://dx.doi.org/10.1063/1.3556707
View Table of Contents: http://scitation.aip.org/content/aip/journal/jcp/134/9?ver=pdfcov
Published by the AIP Publishing

Dynamical mean-field theory from a quantum chemical perspective

Dominika Zgid[a] and Garnet Kin-Lic Chan
Department of Chemistry and Chemical Biology, Cornell University, Ithaca, New York 14853, USA

(Received 16 December 2010; accepted 31 January 2011; published online 7 March 2011)

We investigate the dynamical mean-field theory (DMFT) from a quantum chemical perspective. Dynamical mean-field theory offers a formalism to extend quantum chemical methods for finite systems to infinite periodic problems within a local correlation approximation. In addition, quantum chemical techniques can be used to construct new *ab initio* Hamiltonians and impurity solvers for DMFT. Here, we explore some ways in which these things may be achieved. First, we present an informal overview of dynamical mean-field theory to connect to quantum chemical language. Next, we describe an implementation of dynamical mean-field theory where we start from an *ab initio* Hartree–Fock Hamiltonian that avoids double counting issues present in many applications of DMFT. We then explore the use of the configuration interaction hierarchy in DMFT as an approximate solver for the impurity problem. We also investigate some numerical issues of convergence within DMFT. Our studies are carried out in the context of the cubic hydrogen model, a simple but challenging test for correlation methods. Finally, we finish with some conclusions for future directions.
 [doi:10.1063/1.3556707]

I. INTRODUCTION

In molecular quantum chemistry, the use of systematic hierarchies of electron correlation methods to obtain convergent solutions of the many-electron Schrödinger equation has proven very successful. For example, the hierarchy of second-order Moller-Plesset perturbation theory (MP2), coupled cluster singles doubles theory (CCSD), and coupled cluster singles doubles theory with perturbative triples [CCSD(T)] can be used (when strong correlation effects are absent) to obtain properties of many small molecules with chemical accuracy.[1] The computational scalings of the above methods are respectively n^5, n^6, and n^7, where n is the size of the basis, which seems to limit them to very small systems. However, local correlation techniques can further be used to reduce the above scalings in large systems to n, and this has extended the applicability of such quantum chemical hierarchies to systems with as many as a thousand atoms.[2–5]

Less progress has been made, however, in the use of such quantum chemical hierarchies in infinite systems such as crystalline solids. We recall briefly the reasons why. Consider a molecular crystal, where the molecular unit cell is represented by a basis of n orbitals. Assuming V cells in the Brillouin zone of the crystal, the solid is then represented by a basis of nV orbitals. In density functional theory (computationally a single-electron theory) the cost of the calculation scales as the third power of the number of orbitals. However, translational symmetry means that one-electron operators (such as the Kohn–Sham Hamiltonian) separate into V blocks along the diagonal, and the crystal calculation can be performed for only V times the cost of the molecular calculation, rather than V^3 times, if translational symmetry were absent. In correlated calculations, translational symmetry yields a less dramatic advantage. For example, for second-order Moller–Plesset perturbation theory, while the molecular calculation scales as n^5, the scaling of the crystal calculation with translational symmetry is n^5V^3, and there is still a very steep and prohibitive cost dependence on the size of the Brillouin zone.[6]

Locality of correlation suggests that a formal high scaling with Brillouin zone size can be avoided in physical systems. (Indeed there are many current efforts underway to explore local correlation methods in the crystal setting).[7,8] We can then imagine starting with a different picture of a crystal which is more local in nature. Consider a unit cell in a crystal. It is *embedded in a medium*, namely, the rest of the crystal. Translational symmetry implies that the medium consists of the same unit cells as the embedded cell, and thus an appropriate embedding theory for a crystal should take on a self-consistent nature. If we were to carry out the embedding exactly, we should not expect any less cost than the full crystal calculation. However, if we make the assumption that we will neglect (in some manner) intercell correlations due to locality, then we can expect the high scaling with Brillouin zone size to vanish, since the theory takes on the form of a self-consistent theory for a single unit cell.

Recently, dynamical mean-field theory (DMFT) has been applied with success to strongly correlated crystal problems, which are typically not well described by density functional theory (DFT) or low-order Green's function techniques.[9–16] Note that in this paper, we will use the term DMFT in a general sense, to mean not only the single-site variant but also its cluster and multiorbital extensions.[17] From one perspective, dynamical mean-field theory can be viewed as a framework which realizes the self-consistent embedding with local correlation view of a crystal described above. DMFT is formulated in the language of Green's functions and has the form of a self-consistent theory for the Green's function of a

[a]Author to whom correspondence should be addressed. Electronic mail: dominika.zgid@gmail.com.

unit cell (which may be a primitive cell, or more generally a computational supercell). The local correlation approximation is expressed by assuming that the self-energy is local, i.e., intercell elements of the self-energy vanish, or in momentum space, that the self-energy is momentum independent. It is important to note that although correlation effects are neglected between unit-cells, one-electron delocalization effects between unit cells are included. This, together with the self-consistent nature of the embedding, distinguishes the physics contained in DMFT from that in simpler quantum chemical embedding formalisms, such as theories based on embedding a quantum mechanical cluster into a medium described by molecular mechanics (QM/MM theories).[18] DMFT has some connections in spirit also to density functional embedding methods,[19,20] although the use of Green's functions avoids the need to approximate a nonexplicit nonadditive kinetic energy functional.

There are several ways in which DMFT can benefit the traditional quantum chemical correlation hierarchy and vice versa. (Note that the complementary question, whether or not DMFT can benefit quantum chemistry in finite molecules, is an interesting one. We do not pursue it here, but it has been studied very recently in Ref. 21). First, DMFT provides a framework through which quantum chemical methods for finite systems can be translated to the infinite crystal through the local correlation approximation, avoiding the cost of correlated Brillouin zone sampling. (This is true even for nonsize-extensive methods such as configuration interaction, as one is treating the correlation only within a unit cell and a bath, not the whole crystal simultaneously). The natural way to combine quantum chemical wavefunction methods with DMFT is through the discrete bath formulation of DMFT, where we need to determine the Green's function of a unit cell coupled to a finite noninteracting bath, a so-called impurity problem. Second, quantum chemistry provides systematic ways to treat many-body correlations in the DMFT framework. These quantum chemical solvers are of a different nature to many of the currently used DMFT approximations. Finally, quantum chemical methods and basis sets allow us to define the *ab initio* Hamiltonian and matrix elements needed to carry out DMFT calculations in real systems, while avoiding the empirical parametrization and double counting corrections that are currently part of the DFT-DMFT framework.

The current work can be viewed as taking first steps along some of the lines described above. We aim to do several things in this paper. First, we provide an informal description of DMFT from an embedding perspective. While we do not introduce new ideas in this context, we hope this description may be helpful in forming connections to quantum chemical approximations. Second, we explore quantum chemical wavefunction correlation methods (more specifically, the configuration interaction hierarchy) in the DMFT framework within the discrete bath formulation. These wavefunction methods are used as approximate solvers for the DMFT impurity problem. Third, we define the DMFT Hamiltonian starting from *ab initio* Hartree–Fock theory for the crystal, avoiding any double counting or empirical approximations. (Reference 21 which as mentioned above studies DMFT in the context of molecules, also starts from HF theory to avoid double counting.) Fourth, we explore some of the basic numerics of the DMFT framework, such as the fitting and convergence of the finite bath approximation and the convergence of the self-consistency. We explore all these questions in the context of a simple model system, cubic hydrogen crystal. In such a simple system, the correlation can be tuned from the weak to strong limit as a function of the lattice spacing, and at least in certain regimes, contains correlation features (such as the three peak structure of the density states in the intermediate regime) that to date can only be captured within the DMFT framework.

The structure of the paper is as follows. We begin in Sec. II with an overview of the DMFT formalism, starting with a recap of relevant theory of Green's functions, then proceeding to a general discussion of DMFT self-consistency and embedding, the formulation of the impurity problem and the many-body solver, and the definition of the DMFT Hamiltonian starting from Hartree–Fock theory to avoid double counting. Sec. III summarizes our implementation of the DMFT algorithm. Section IV describes our exploration of several aspects of the combination of DMFT and quantum chemistry methods and DMFT numerics in the cubic hydrogen system, including the use of the configuration interaction hierarchy as a solver, the convergence of the DMFT self-consistency, and the convergence of the DMFT calculations as a function of the bath size. We present our conclusions in Sec. V.

II. AN INFORMAL OVERVIEW OF DMFT

A. Summary of Green's function formalism

To keep our discussion self-contained and to establish notation, we begin by recalling some of the basic results from the theory of Green's functions. More detailed exposition of Green's functions can be found, for example, in Ref. 22. Given a Hamiltonian H and chemical potential μ, at zero-temperature the Green's function $\mathbf{G}(\omega)$ is defined as

$$G_{ij}(\omega) = \langle \Psi_0 | a_i \frac{1}{\omega + \mu - (H - E_0) + i0} a_j^\dagger | \Psi_0 \rangle + \langle \Psi_0 | a_j^\dagger \frac{1}{\omega + \mu + (H - E_0) - i0} a_i | \Psi_0 \rangle, \quad (1)$$

where i, j label the orthogonal one-particle basis, and Ψ_0 and E_0 are the ground-state eigenfunction and eigenvalue of H, respectively. $\mathbf{G}(\omega)$ explicitly determines many of the interesting properties of the system. For example the single-particle density matrix $\mathbf{P}$, electronic energy E, and spectral function (density of states) $\mathbf{A}(\omega)$ are given, respectively, by

$$\mathbf{P} = -i \int_{-\infty}^{\infty} e^{i\omega 0_+} \mathbf{G}(\omega) d\omega, \quad (2)$$

$$E = -\frac{1}{2} i \int_{-\infty}^{\infty} e^{i\omega 0_+} \mathrm{Tr}[(\mathbf{h} + \omega)\mathbf{G}(\omega)] d\omega, \quad (3)$$

$$\mathbf{A}(\omega) = -\frac{1}{\pi} \Im \mathbf{G}(\omega + i0_+). \quad (4)$$

In general, ω is a complex variable. Real ω corresponds to physical frequencies, and for example, the density of states

(4) is defined on the real axis. However, it is often more convenient to work away from the real axis. For example, expectation values such as Eqs. (2) and (3) should be evaluated on contours away from the real axis to avoid singularities in the numerical integration.

In a crystal, we assume a localized orthogonal one-particle basis of dimension n in each unit cell. Using translational invariance, it is sufficient to write the Green's function as $\mathbf{G}(\mathbf{R}, \omega)$, where $\mathbf{R}$ is the translation vector between unit cells and for each $\mathbf{R}$, ω, $\mathbf{G}(\mathbf{R}, \omega)$ is an $n \times n$ matrix. We shall often refer to the Green's function of a unit cell in this work as the *local* Green's function. The local Green's function is then the block of $\mathbf{G}(\mathbf{R}, \omega)$ at the origin $\mathbf{R} = 0$, and we denote this by $\mathbf{G}(\mathbf{R}_0, \omega)$. The local Green's function determines the local observables, such as the density matrix of the unit cell, or the local density of states, via formulas analogous to Eqs. (2) and (4). With periodicity, we can also work in the reciprocal k-space. The k-space Green's function $\mathbf{G}(\mathbf{k}, \omega)$ is defined from the Fourier transform,

$$\mathbf{G}(\mathbf{k}, \omega) = \sum_{\mathbf{R}} \mathbf{G}(\mathbf{R}, \omega) \exp(i\mathbf{k} \cdot \mathbf{R}), \tag{5}$$

and the local Green's function is obtained from the inverse transform as

$$\mathbf{G}(\mathbf{R}_0, \omega) = \frac{1}{V} \sum_{\mathbf{k}} \mathbf{G}(\mathbf{k}, \omega), \tag{6}$$

where V is the volume of the Brillouin zone.

When the finite system Hamiltonian is of single particle form, $h = \sum_{ij} h_{ij} a_i^\dagger a_j$, the corresponding noninteracting Green's function is obtained from the one-electron matrix $\mathbf{h}$ as

$$\mathbf{g}(\omega) = [(\omega + \mu + i0_\pm)\mathbf{1} - \mathbf{h}]^{-1}, \tag{7}$$

where we use the convention of lower case $\mathbf{g}(\omega)$ and $\mathbf{h}(\omega)$ to denote quantities associated with a noninteracting problem, and the infinitesimal broadening $0_\pm$ is positive or negative depending on the sign of ω. In a periodic crystal, we obtain the noninteracting Green's function in k-space from the k-space Hamiltonian $\mathbf{h}(\mathbf{k})$ for each k point,

$$\mathbf{g}(\mathbf{k}, \omega) = [(\omega + \mu + i0_\pm)\mathbf{1} - \mathbf{h}(\mathbf{k})]^{-1}. \tag{8}$$

Green's functions $\mathbf{G}(\omega)$, $\mathbf{G}'(\omega)$ corresponding to different Hamiltonians $\mathbf{H}$, $\mathbf{H}'$ are related through frequency dependent one-particle potentials termed self-energies. The self-energy $\mathbf{\Sigma}(\omega)$ is defined via the Dyson equation as

$$\mathbf{\Sigma}(\omega) = \mathbf{G}'^{-1}(\omega) - \mathbf{G}^{-1}(\omega). \tag{9}$$

It contains all the physical effects associated with the perturbation $\mathbf{H}' - \mathbf{H}$. For example, we can exactly relate the noninteracting Green's function $\mathbf{g}(\omega)$ from Eq. (7) associated with noninteracting Hamiltonian $\mathbf{h}$, and the interacting Green's function $\mathbf{G}(\omega)$ associated with interacting Hamiltonian $\mathbf{H}$ through a Coulombic self-energy. From the explicit form of the noninteracting Green's function $\mathbf{g}(\omega)$, the Dyson equation in this case is

$$\mathbf{G}^{-1}(\omega) = (\omega + \mu + i0_\pm)\mathbf{1} - \mathbf{h} - \Sigma(\omega). \tag{10}$$

In a periodic system, the above equation holds at each k where the self-energy $\mathbf{\Sigma}(\mathbf{k}, \omega)$ now also acquires a k-dependence,

$$\mathbf{G}^{-1}(\mathbf{k}, \omega) = (\omega + \mu + i0_\pm)\mathbf{1} - \mathbf{h}(\mathbf{k}) - \Sigma(\mathbf{k}, \omega), \tag{11}$$

and the local Green's function becomes

$$\mathbf{G}(\mathbf{R}_0, \omega) = \frac{1}{V} \sum_{\mathbf{k}} [(\omega + \mu + i0_\pm)\mathbf{1} - \mathbf{h}(\mathbf{k}) - \mathbf{\Sigma}(\mathbf{k}, \omega)]^{-1}. \tag{12}$$

In general, it is convenient to relax the assumption of orthogonality of the one-particle basis, for example, to work with an atomic orbital basis. For this, the unit matrix $\mathbf{1}$ in the above formulas should be replaced by a general overlap matrix $\mathbf{S}$, e.g., Eq. (12) becomes

$$\mathbf{G}(\mathbf{R}_0, \omega) = \frac{1}{V} \sum_{\mathbf{k}} [(\omega + \mu + i0_\pm)\mathbf{S}(\mathbf{k}) - \mathbf{h}(\mathbf{k}) - \mathbf{\Sigma}(\mathbf{k}, \omega)]^{-1}. \tag{13}$$

In addition expectation values must be suitably modified. For example, the local spectral function $\mathbf{A}(\mathbf{R}_0, \omega)$ is given by

$$\mathbf{A}(\mathbf{R}_0, \omega) = \frac{1}{V} \Im \sum_{\mathbf{k}} \mathbf{G}(\mathbf{k}, \omega + i0_+)\mathbf{S}(\mathbf{k}). \tag{14}$$

As our calculations in this work use a nonorthogonal basis, we will henceforth use expressions with explicit overlap dependence.

B. DMFT equations

In DMFT, the central quantity is the local Green's function $\mathbf{G}(\mathbf{R}_0, \omega)$ (the Green's function of the unit cell) which is determined in a self-consistent way, including the embedding effects of the crystal within a local self-energy (correlation) assumption. Here, we describe how the DMFT framework and the local self-energy assumption and self-consistency are established. Of course, we recommend that the reader also consult one of the many excellent review articles for further discussion and illumination of the DMFT formalism.[9,11–13,15]

From Eq. (13), we observe that $\mathbf{G}(\mathbf{R}_0, \omega)$ can be calculated if we have the exact Coulomb self-energy $\mathbf{\Sigma}(\mathbf{k}, \omega)$. However, determining $\mathbf{\Sigma}(\mathbf{k}, \omega)$ requires solving the many-body problem for the whole crystal. Thus, the idea in DMFT is to approximate $\mathbf{\Sigma}(\mathbf{k}, \omega)$ by one of its main components, the local self-energy $\mathbf{\Sigma}(\omega)$, in essence, a local correlation approximation. Formally, this is the contribution to the self-energy of skeleton diagrams in the Green's function perturbation theory where the Coulomb interaction has all local indices, i.e., all indices local to a single unit cell. The DMFT approximation neglects the k-dependence of the self-energy. In real-space, this corresponds to neglecting off-diagonal terms of the self-energy between unit cells. The local approximation is plausible due to the local nature of correlation, and in fact as the physical dimension or local coordination number $D \to \infty$, the approximation becomes exact.[11] With the DMFT local approximation, the local Green's function defined in Eq. (6) is

simply

$$\mathbf{G}(\mathbf{R}_0, \omega) = \frac{1}{V}\sum_{\mathbf{k}}[(\omega + \mu + i0_{\pm})\mathbf{S}(\mathbf{k}) - \mathbf{h}(\mathbf{k}) - \mathbf{\Sigma}(\omega)]^{-1}. \tag{15}$$

Now, $\mathbf{\Sigma}(\omega)$ is formally defined by contributions of only the local Coulomb interaction to the local Green's function. However, this is still a many-body problem. In DMFT, we usually reformulate the determination of $\mathbf{\Sigma}(\omega)$ in terms of the many-body solution of an embedded, or *impurity*, problem, where we view the unit cell as an impurity embedded in a bath of the surrounding crystal. (The impurity nomenclature originates from impurity problems in condensed matter such as the Kondo and Anderson models, which informed some of the early work in DMFT). Within this impurity mapping, the many-body determination of the Green's function of the embedded unit cell or impurity Green's function $\mathbf{G}_{imp}(\omega)$ defines the local self-energy $\mathbf{\Sigma}(\omega)$.

We discuss the impurity problem and impurity solvers to obtain the self-energy, in more detail in Sec. II C. We focus for now on how the self-consistent embedding is established in DMFT. For the theory to be consistent, the impurity Green's function (i.e., the Green's function of the embedded unit cell in the impurity model) should be equivalent to the actual local Green's function of the crystal, at least within the local self-energy approximation. This means at self-consistency

$$\mathbf{G}_{imp}(\omega) = \mathbf{G}(\mathbf{R}_0, \omega). \tag{16}$$

The embedding to achieve the equality (16) can be enforced through an embedding self-energy, the hybridization $\mathbf{\Delta}(\omega)$. The Dyson equation relating the impurity Green's function and the self-energy and hybridization is then

$$\mathbf{G}_{imp}(\omega)^{-1} = (\omega + \mu + i0_{\pm})\mathbf{S} - \mathbf{h}_{imp} - \mathbf{\Sigma}(\omega) - \mathbf{\Delta}(\omega), \tag{17}$$

where h_{imp} is a one-electron Hamiltonian in the unit cell. Once we have solved the many-body impurity problem to obtain $\mathbf{G}_{imp}$, Eq. (17) defines the local self-energy through

$$\mathbf{\Sigma}(\omega) = (\omega + \mu + i0_{\pm})\mathbf{S} - \mathbf{h}_{imp} - \mathbf{\Delta}(\omega) - \mathbf{G}_{imp}(\omega)^{-1}. \tag{18}$$

The hybridization $\mathbf{\Delta}(\omega)$ can also be defined through a similar equation from the local Green's function, obtained from Eq. (15),

$$\mathbf{\Delta}(\omega) = (\omega + \mu + i0_{\pm})\mathbf{S} - \mathbf{h}_{imp} - \mathbf{\Sigma}(\omega) - \mathbf{G}(\mathbf{R}_0, \omega)^{-1}. \tag{19}$$

Schematically therefore, for a given hybridization $\mathbf{\Delta}(\omega)$, solution of the impurity problem yields $\mathbf{G}_{imp}(\omega)$ and the local self-energy $\mathbf{\Sigma}(\omega)$,

$$\mathbf{\Delta}(\omega) \overset{\text{impurity solver}}{\rightarrow} \mathbf{G}_{imp}(\omega) \rightarrow \mathbf{\Sigma}(\omega), \tag{20}$$

while given the local self-energy, Eq. (15) yields the local Green's function and the hybridization

$$\mathbf{\Sigma}(\omega) \rightarrow \mathbf{G}(\mathbf{k}, \omega) \rightarrow \mathbf{G}(\mathbf{R}_0, \omega) \rightarrow \mathbf{\Delta}(\omega). \tag{21}$$

Equations (21) and (20) thus form a self-consistent pair of equations for the self-energy and hybridization that should be iterated to convergence. These are the DMFT self-consistent equations. At the solution point, the impurity Green's function and local Green's function, are identical as in Eq. (16).

We note here that the Green's functions $\mathbf{G}(\mathbf{R}_0, \omega)$, $\mathbf{G}_{imp}(\omega)$, and the self-energy and hybridization $\mathbf{\Sigma}(\omega)$, $\mathbf{\Delta}(\omega)$ are smooth functions away from the real axis. For this reason, the impurity problem and the numerical implementation of self-consistency are always considered on the imaginary axis rather than the real axis. Once the self-consistency Eq. (16) has been reached on the imaginary axis, analyticity guarantees equivalence of the Green's functions in the whole complex plane. One can then use the converged $\mathbf{\Delta}(\omega)$ (continued to the real axis) to recalculate properties along the real axis, such as spectral functions, as needed. (Many quantities, such as density matrices, require only information along the imaginary axis, however).

We recap the main physical effects contained within the DMFT treatment—local Coulomb interaction effects are included in each unit cell and replicated throughout the crystal in a self-consistent way, which takes into account the embedding of each unit cell in an environment of the others. Long-range Coulomb terms are not included in the theory, although they can be systematically added. In Sec. II D, we describe how the long-range terms can be treated at the mean-field level.

Note that we have assumed in the above that we are working at a fixed μ. Normally, however, we are interested not in fixed μ, but in some fixed particle number of the crystal per unit cell, $N_0(\mathbf{R}_0)$. As $\mathbf{\Sigma}(\omega)$ changes, $N(\mathbf{R}_0)$, the current particle number in the crystal unit cell, given by [using Eqs. (2) and (15)]

$$N(\mathbf{R}_0) = -\frac{i}{V}\int_{-\infty}^{\infty} e^{i\omega 0_+}\mathrm{Tr} \times\left[\sum_k \mathbf{S}(\mathbf{k})[(\omega+\mu+i0_{\pm})\mathbf{S}(\mathbf{k})-\mathbf{h}(\mathbf{k})-\mathbf{\Sigma}(\omega)]^{-1}\right]d\omega \tag{22}$$

will change. Thus together with the self-consistency, the chemical potential μ must be adjusted such that $N(\mathbf{R}_0) = N_0(\mathbf{R}_0)$. The full DMFT algorithm to do so is summarized in Sec. III.

We now turn to consider the many-body impurity problem and methods for its solution.

C. The impurity problem and solver in the discrete bath formulation

The purpose of the impurity formulation is to obtain an impurity Green's function $\mathbf{G}_{imp}(\omega)$ and a corresponding self-energy $\mathbf{\Sigma}(\omega)$ that describes the effects of the local Coulomb interaction in the presence of the hybridization $\mathbf{\Delta}(\omega)$. In general, due to its many-body nature, the impurity problem cannot be solved exactly. The approximate method used to solve the impurity problem is known as the impurity solver.

There are two formulations in which an impurity solver can work.[11] In the first one the impurity Green's function is expressed as a functional integral, and its determination is a problem of high-dimensional integration. This is typically performed using Monte Carlo methods such as Hirsch–Fye[23]

or continuous time quantum Monte Carlo methods.[24–27] In this formulation, the bath is infinite and one does not deal with it explicitly since it can be integrated out thus avoiding any bath discretization error. These methods are powerful but suffer in general from a sign problem, as well as difficulties in obtaining quantities on the real frequency axis (such as the spectral function) which requires analytic continuation. We will not discuss the Monte Carlo formulations of the solver further here, but we refer the reader to an excellent review.[28]

The second formulation describes an impurity model with an explicit finite, discrete bath. Here the idea is to view the hybridization $\mathbf{\Delta}(\omega)$ as arising from a one-electron coupling between the impurity orbitals (orbitals of the unit cell) and a fictitious finite noninteracting bath. The relevance of the formulation with discrete bath here is that the determination of the impurity Green's function reduces to the determination of the Green's function of a finite problem, and this can be tackled using standard quantum chemistry wavefunction techniques, which avoid the sign problem encountered in Monte Carlo based solvers. We can view then such an discrete bath formulation as providing a way to extend quantum chemical methods for finite systems to treat the infinite crystal, within the DMFT approximation of a local self-energy.

Denoting the local orbitals by $i, j, \ldots$, and bath orbitals by $p, q \ldots$, we can write an impurity Hamiltonian for the impurity orbitals and the fictitious noninteracting bath as

$$H_{imp+bath} = \sum_{ij} t_{ij} a_i^\dagger a_j + \frac{1}{2}\sum_{ijkl} w_{ijkl} a_i^\dagger a_j^\dagger a_l a_k + \sum_{ip} V_{ip}(a_i^\dagger a_p + a_p^\dagger a_i) + \sum_p \epsilon_p a_p^\dagger a_p. \quad (23)$$

The noninteracting bath yields a hybridization $\mathbf{\Delta}(\omega)$ for the impurity orbitals of the form

$$\Delta_{ij}(\omega) = \sum_p \frac{V_{ip}^* V_{jp}}{\omega - \epsilon_p}. \quad (24)$$

In general, we assume that physical $\mathbf{\Delta}(\omega)$ can be approximately represented in terms of the noninteracting bath by fitting the couplings V and the energies ϵ, and this is generally found to be true. This resembles the assumption of noninteracting v-representability of the density in density functional theory. Fortunately, the convergence of (24) with respect to the number of bath orbitals is quite rapid; one does not need a bath the size of the entire crystal to obtain a good representation of the hybridization. (Recall that the fit to the bath is always carried out on the imaginary frequency axis, where $\mathbf{\Delta}(\omega)$ is very smooth).

The form of the bath hybridization in Eq. (24) requires that $\lim_{\omega\to\infty} \mathbf{\Delta}(\omega) \to 0$. While this is true of physical hybridizations in an orthogonal basis, the case of a nonorthogonal basis requires a little more care, as discussed for example, in Ref. 15. Rearranging Eq. (17) and inserting the definition of the local Green's function, we see that the hybridization is given by

$$\mathbf{\Delta}(\omega) = (\omega + \mu + i0_+)\mathbf{S}_{imp} - \mathbf{h}_{imp} - \mathbf{\Sigma}(\omega) - \mathbf{G}(\mathbf{R}_0, \omega)^{-1}. \quad (25)$$

The definition of the impurity overlap matrix $\mathbf{S}_{imp}$ and impurity one-electron Hamiltonian $\mathbf{h}_{imp}$ can be viewed as adjustable as the equality of the impurity Greens function and local crystal Green's function, can be maintained through appropriate definitions of the hybridization and self-energy in Eq. (17). Consequently, we choose $\mathbf{S}_{imp}$ and $\mathbf{h}_{imp}$ to ensure that the hybridization can be represented by the form Eq. (24). Expanding the denominator in powers of $1/\omega$, we find that to ensure $\mathbf{\Delta}(\omega)$ vanishes like $1/\omega$, we should define the impurity overlap and one-electron Hamiltonian as[15]

$$\mathbf{S}_{imp} = \left[\frac{1}{V}\sum_{\mathbf{k}} \mathbf{S}^{-1}(\mathbf{k})\right]^{-1}, \quad (26)$$

$$\mathbf{h}_{imp} = \mathbf{S}_{imp}\left[\sum_{\mathbf{k}} \mathbf{S}^{-1}(\mathbf{k})[\mathbf{h}(\mathbf{k}) + \mathbf{\Sigma}_\infty]\mathbf{S}^{-1}(\mathbf{k})\right]\mathbf{S}_{imp} - \mathbf{\Sigma}_\infty, \quad (27)$$

where $\mathbf{\Sigma}_\infty = \mathbf{\Sigma}(\infty)$.

Now that we have defined a finite Hamiltonian for the impurity and a finite bath, the determination of the impurity Green's function $\mathbf{G}_{imp}(\omega)$ is the determination of the Green's function of a finite problem. $\mathbf{G}_{imp}(\omega)$ is defined through Eq. (1) with the impurity Hamiltonian,

$$G_{ij}(\omega) = \langle\Psi_0|a_i \frac{1}{\omega+\mu-(H_{imp+bath}-E_{imp+bath})+i0} a_j^\dagger|\Psi_0\rangle + \langle\Psi_0|a_j^\dagger \frac{1}{\omega+\mu+(H_{imp+bath}-E_{imp+bath})-i0} a_i|\Psi_0\rangle, \quad (28)$$

where i, j denote the impurity orbitals, i.e., the local orbitals of the unit cell, and $E_{imp+bath}$, Ψ_0 are the ground-state eigenvalue and eigenfunction of $H_{imp+bath}$. Both Ψ_0 and the corresponding $\mathbf{G}_{imp}(\omega)$ can be determined through wavefunction techniques familiar in quantum chemistry.

One subtlety is that the finite problem Ψ_0 is determined for some fixed particle number $N_{imp+bath}$ (and spin, say). In principle, at zero temperature, we should use the $N_{imp+bath}^{min}$ (and spin) which minimizes $E_{imp+bath}$ for the given chemical potential μ. This means that we have to carry out a search over these quantum numbers. Of course μ and $\mathbf{\Delta}(\omega)$ are also changing in the DMFT iterations, and thus in the discrete bath formulation, the impurity model is a function of $N_{imp+bath}$ (and other quantum numbers), μ, and $\mathbf{\Delta}(\omega)$. The structure of the full self-consistency involving these variables is summarized in the DMFT algorithm in Sec. III.

A popular approach in existing DMFT applications is to use full configuration interaction (FCI) called exact diagonalization (ED) in solid state physics community to solve for Ψ_0 and $\mathbf{G}_{imp}(\omega)$.[11,29] From a DMFT perspective, the advantage of this approach compared to Monte Carlo techniques is that it provides direct access to the calculation of the Green's function on the real axis, and consequently the spectral function, without the need to perform analytic continuation as is used in Monte Carlo solvers. In addition,

there is no sign problem. However, FCI is naturally limited to very small numbers of impurity and bath orbitals, and the cost of evaluating the Green's function (typically at several hundred frequencies) means that such calculations are orders of magnitude more expensive than typical ground-state FCI calculations for molecules. One way to avoid this limitation is to employ the various systematic quantum chemistry wavefunction hierarchies as impurity solvers. We will investigate one such simple approximate solver, the configuration interaction hierarchy, in Sec. IV B.

D. Eliminating double counting in DMFT through Hartree–Fock theory

In current applications of DMFT to real materials, it is common to combine DMFT with a density functional derived Hamiltonian, the so-called DFT-DMFT approximation.[12,13,15] Within this formalism, one does not work with a strict *ab initio* Hamiltonian, but rather with a model Hamiltonian,

$$H_{imp} = H_{DFT} + \frac{1}{2}\sum_{ijkl\in act} w_{ijkl} a_i^\dagger a_j^\dagger a_l a_k - H_{d.c.}, \quad (29)$$

where H_{DFT} is the sum of one-electron Kohn–Sham operators and $H_{d.c.}$ is a double-counting correction (see below). The two electron interaction w_{ijkl} is chosen to sum over a set of active orbitals in the computational unit cell. In transition metal applications, these are usually a minimal basis of d or f valence orbitals, the idea being that the Coulomb interaction in these orbitals should be treated with the explicitly many-body DMFT framework, rather than within a DFT functional. While w_{ijkl} may be obtained from *ab initio* Coulomb integrals[30,31] or derived via, e.g., constrained DFT calculations,[32,33] they are best regarded in this approach as semi-empirical parameters. The advantage of using DMFT in only an active space is that delocalized, itinerant electrons are well treated by existing exchange-correlation functionals and not well-treated within the DMFT framework which neglects nonlocal correlations, while the many-body DMFT framework allows a systematic approach to high order strong correlations in the d and f shells. The adjustment of w_{ijkl} further allows one to account for effective screening of the active space Coulomb matrix elements by long-range correlations. The DFT-DMFT approach has been successful in reproducing many properties of strongly correlated materials and an excellent description of the possible applications and the way of dealing with the double counting correction can be found in Refs. 12, 13, and 34. However, there are obvious drawbacks. In particular, the Hamiltonian may be considered to be uncontrolled on two levels. First, since exchange-correlation effects in DFT are not separated between different orbitals, there is a double counting of the Coulomb interaction in H_{DFT} and w. This is the origin of the double-counting correction $H_{d.c.}$, which must be adjusted empirically. The double counting problem is similar to that encountered in molecular quantum chemistry when DFT is combined with active space wave function methods.[35] Second, the use of a parametrized form for w_{ijkl} must also be regarded as unsystematic.

In the current work, we take a more quantum chemical approach to DMFT where we try to retain a strict diagrammatic control over the approximations made. This can be achieved by starting with a Hartree–Fock description of the crystal. Within each unit cell we identify an active space, typically a set of localized atomic orbitals. (In fact, in the application to cubic hydrogen in this work, all the orbitals in the unit cell will be active). Then, we use DMFT to treat the active space Coulomb interaction while the remaining Coulomb interactions (e.g., long-range Coulomb interactions between unit cells, as well the interactions between the active and inactive orbitals) are treated through the Hartree–Fock mean-field. The Hamiltonian in the active space treated within DMFT therefore takes the form

$$H_{imp} = \sum_{ij\in act} (f_{ij} - \tilde{f}_{ij}) a_i^\dagger a_j + \frac{1}{2}\sum_{ijkl\in act} w_{ijkl} a_i^\dagger a_j^\dagger a_k a_l, \quad (30)$$

where the $\tilde{f}_{ij}$ terms represents the exact subtraction of the active-space Hartree–Fock density matrix $\mathbf{P}^{HF}$, contribution to the mean-field Coulomb treatment,

$$\tilde{f}_{ij} = \sum_{kl\in act} P_{kl}^{HF}(w_{iklj} - w_{ilkj}). \quad (31)$$

This subtraction exactly eliminates any double counting between the mean-field and DMFT treatments. Note that while the inactive Coulomb interactions (such as the long-range Coulomb interactions) are only treated at the Hartree–Fock level (which is a severe approximation in many solids) the mean-field treatment may be viewed as the lowest level of a hierarchy of perturbation treatments of these interactions and is thus systematically improvable. Reference 21 also explores a Hartree–Fock starting point to avoid double counting, but in the context of DMFT applied to finite systems.

III. DMFT ALGORITHM

We now summarize the DMFT algorithm in our current implementation, following the basic ideas outlined in the earlier sections. We have implemented our algorithm in a custom code that interfaces to the CRYSTAL Gaussian based periodic code[36] as well as the DALTON molecular code.[37] We recall that within the formulation with discrete bath, the impurity model is defined as a function of three variables: $N_{imp+bath}$ (particle number of the impurity model), μ (chemical potential), and the hybridization $\mathbf{\Delta}(\omega)$ which defines a bath parametrization. All three have to be determined self-consistently together. At the solution point of the DMFT algorithm, $N_{imp+bath}$ minimizes the ground-state energy of the impurity model $E_{imp+bath}$ (Sec. II C), μ yields the correct particle number per unit cell of the crystal $N(\mathbf{R_0})$ [Eq. (22)], and $\mathbf{\Delta}(\omega)$ satisfies the DMFT self-consistency conditions (20), (21). The high-level loop structure of the algorithm is summarized in ALGORITHM I. The individual steps are

ALGORITHM I. General DMFT loop structure. Note that the DMFT self-consistency is carried out on the imaginary frequency axis.

1: **for all** $N_{imp+bath}$ **do**
2: **while** $N(\mathbf{R}_0) \neq N_0(\mathbf{R}_0)$ **do**
3: Choose new μ (e.g., by bisection)
4: Perform DMFT self-consistency for $\mathbf{\Sigma}(\omega)$, $\mathbf{\Delta}(\omega)$.
5: Calculate $E_{imp+bath}$
6: Calculate $N(\mathbf{R}_0)$
7: **end while**
8: **end for**
9: Choose $N^{min}_{imp+bath}$ that minimizes $E_{imp+bath}$
10: For $N^{min}_{imp+bath}$ and the corresponding μ, $\mathbf{\Delta}(\omega)$ and impurity model, calculate $\mathbf{G}(\mathbf{R_0}, \omega)$ including quantities on the real axis, e.g., spectral functions

ALGORITHM II. DMFT self-consistency for $\mathbf{\Delta}(\omega)$, $\mathbf{\Sigma}(\omega)$. Note that all calculations are done on the imaginary frequency axis.

1: Obtain Hartree–Fock Fock matrix $\mathbf{f}(\mathbf{k})$, overlap matrix $\mathbf{S}(\mathbf{k})$, density matrix $\mathbf{P}(\mathbf{R}_0)$, and initial guess for $\mathbf{\Delta}(\omega)$.
2: **while** $||\mathbf{\Sigma}(\omega) - \mathbf{\Sigma}^{old}(\omega)|| > \tau$ **do**
3: Construct Hamiltonian for impurity orbitals with overlap correction (using $\mathbf{\Sigma}(\infty)$)
4: Construct bath representation from $\mathbf{\Delta}(\omega)$
5: Calculate impurity Greens function and new self-energy $\mathbf{\Sigma}(\omega)$
6: Update self-energy $\mathbf{\Sigma}(\omega)$, $\mathbf{\Sigma}^{old}(\omega)$
7: Update $\mathbf{\Delta}(\omega)$
8: **end while**

1. Loop over possible particle numbers $N_{imp+bath}$ of the impurity model [to determine $N_{imp+bath}$ which minimizes the impurity model energy $E_{imp+bath}(N_{imp+bath})$]. (In principle we should search over spin, but we do not do this is in general in our applications here).
2. For each $N_{imp+bath}$, search over chemical potential μ (e.g., by bisection) to satisfy the crystal unit cell particle number constraint $N(\mathbf{R_0}) = N_0(\mathbf{R_0})$.

3–6. For given μ, $N_{imp+bath}$, carry out the DMFT self-consistent loop to determine $\mathbf{\Sigma}(\omega)$, $\mathbf{\Delta}(\omega)$ and the impurity ground state energy $E_{imp+bath}$. Note that all calculations are here done on the imaginary frequency axis.

9–10. Determine $N_{imp+bath}$ which led to the lowest $E_{imp+bath}$. Using the corresponding μ and hybridization parametrization, which satisfy the crystal particle number constraint and the DMFT self-energy self-consistency equations, recalculate the local Greens function $G(\mathbf{R}_0, \omega)$ and other desired observables, e.g., the local spectral function $\mathbf{A}(\omega)$ along the real axis.

The DMFT self-consistent loop for $\mathbf{\Sigma}(\omega)$, $\mathbf{\Delta}(\omega)$ constitutes the core part of the algorithm. It is summarized in ALGORITHM II. The individual steps are

1. Initialization. Perform a HF calculation on the crystal in a local basis. Extract the converged Fock matrix $\mathbf{f}(\mathbf{k})$ and overlap matrix $\mathbf{S}(\mathbf{k})$ in k-space, and the Hartree–Fock unit-cell density matrix $\mathbf{P}(\mathbf{R}_0)$. The k-space Fock and overlap matrices are then used to construct their real-space analogs in the unit-cell.
2. Begin DMFT self-consistent loop until convergence in the self-energy (to within a threshold τ) is reached.
3. Impurity Hamiltonian construction. Construct the impurity orbital part of the Hamiltonian. The two-body integrals w_{ijkl} are computed in the same local basis as used in the crystal calculation. The one-body Hamiltonian for the impurity orbitals $\mathbf{h}_{imp}$ is defined as in Eq. (31) using the exact subtraction of the mean-field Coulomb treatment, i.e., $\mathbf{h}_{imp} = \mathbf{f}(\mathbf{R}_0) - \tilde{\mathbf{f}}(\mathbf{R}_0)$, while the overlap of the impurity orbitals is taken as the overlap in the unit-cell, $\mathbf{S}_{imp} = \mathbf{S}(\mathbf{R}_0)$. Finally, $\mathbf{h}_{imp}$ and $\mathbf{S}_{imp}$ are corrected as in Eqs. (26) and (27).
4. Bath construction. From the hybridization $\mathbf{\Delta}(\omega)$, obtain the bath Hamiltonian parametrization by fitting. In the first iteration, the hybridization is fitted to the Hartree–Fock hybridization, defined as

$$\mathbf{\Delta}^{HF}(\omega) = (\omega + \mu + i0_{\pm})\mathbf{S}_{imp} - \mathbf{h}_{imp} + \\ - \left[\frac{1}{V}\sum_{k}(\omega + \mu + i0_{\pm})\mathbf{S}(\mathbf{k}) - \mathbf{f}(\mathbf{k})\right]^{-1}. \quad (32)$$

This provides a good guess for the DMFT algorithm. Further details of the bath fitting algorithm are given in Sec. IV D and in the Appendix.

5. Calculate the ground-state wavefunction of the impurity problem (for given $N_{imp+bath}$). Then calculate the impurity Green's function on the imaginary axis using a truncated configuration interaction solver, described in Sec. IV B.

6–7. Update the self-energy $\mathbf{\Sigma}(\omega)$ and hybridization $\mathbf{\Delta}(\omega)$ defined through Eqs. (9) and (19). For better convergence, the self-energy is updated in a damped fashion, $\mathbf{\Sigma}(\omega) \leftarrow (1-\alpha)\mathbf{\Sigma}(\omega) + \alpha\mathbf{\Sigma}^{old}(\omega)$, where $0 < \alpha < 1$.

IV. BENCHMARK DMFT STUDIES

We now proceed to our benchmark DMFT studies. In particular, we investigate the following:

1. The preliminary combination of quantum chemical and DMFT ideas, using the configuration interaction (CI) hierarchy as a solver for the DMFT impurity problem (or conversely, using DMFT to extend truncated CI variants to treat the infinite crystal), starting from an *ab initio* Hartree–Fock DMFT Hamiltonian.
2. The numerical behavior of the DMFT algorithm, including convergence of the self-consistency cycle, fitting the hybridization by a finite bath, and convergence of correlated properties (such as spectral functions) as a function of bath size. We should stress that similar studies were caried out before using FCI called ED in solid state physics community. Here, however, we will focus on using the truncated version of configuration interaction as a solver that was developed by us and examine with it

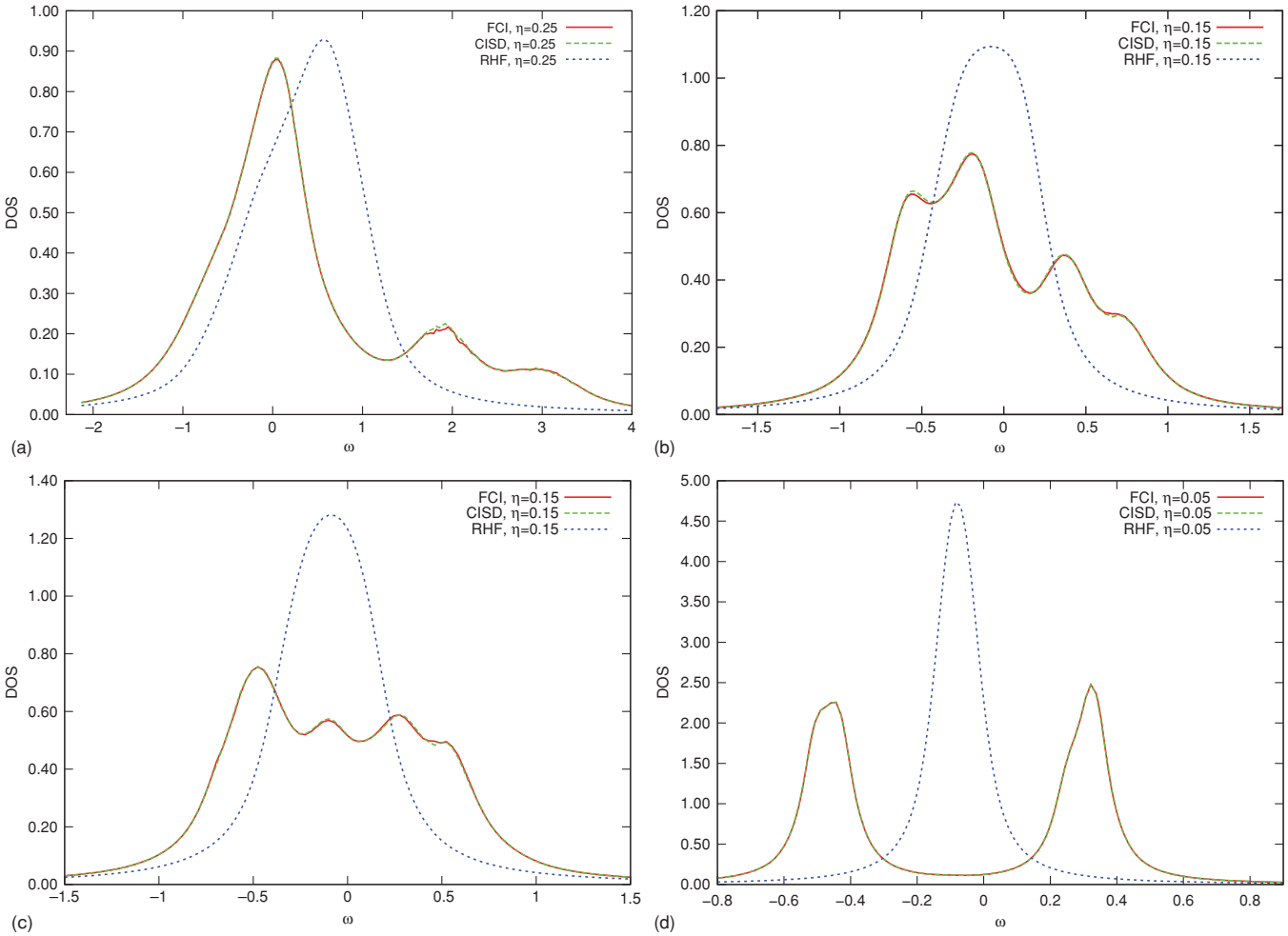

FIG. 1. Spectral functions (density of states) from FCI, CISD, and RHF calculations for cubic hydrogen, at various lattice constants. **(A)** $a_0 = 1.40$ Å, 9 bath orbitals, 300 frequency points. **(B)** $a_0 = 2.25$ Å, 9 bath orbitals, 300 frequency points. **(C)** $a_0 = 2.50$ Å, 9 bath orbitals, 300 frequency points. **(D)** $a_0 = 6.00$ Å, 9 bath orbitals, 300 frequency points.

the questions of interest concerning the numerics of the DMFT algorithm.

Our studies are carried out on an idealized test system, namely (three-dimensional) cubic hydrogen. Hydrogen clusters in 1, 2, and 3-dimensions have been popular models in the study of correlation effects in quantum chemistry, as the correlation can be tuned from the weak to the strong regime as the lattice spacing is increased.[38,39] Here, we study only cubic hydrogen (i.e., three dimensions). We use a minimal basis (STO-3G) and a unit cell with a single hydrogen atom, and the initial Hartree–Fock crystal calculations are carried out using the Gaussian based periodic code CRYSTAL .[36] The use of a Gaussian basis means that we employ the general nonorthogonal formulation for the Green's function quantities in Sec. II A, as well as the overlap corrections to the impurity model Hamiltonian and overlap in Sec. II C. Note that the impurity problem in this case has only a single 1*s* impurity orbital, and the local Green's function also only has a single orbital index.

We begin with a brief overview of the properties of the DMFT solution of the cubic hydrogen model before proceeding to discuss the areas above.

A. The cubic hydrogen solid model

We have carried out DMFT calculations on the cubic hydrogen model for a variety of lattice constants. We find that cubic hydrogen exhibits three electronic regimes as a function of lattice spacing which are well-known from analogous DMFT studies of Hubbard models.[10,11,14,40,41] We first summarize the main features of the spectral functions and the impurity wavefunctions. [The spectral functions plotted here are defined as the trace of the local spectral function in Eq. (14)]. The regimes are

- *Metallic* regime. This occurs with lattice constants near equilibrium, and is illustrated by calculations at lattice constant 1.4 Å. The spectral function displays a single broad peak, indicative of metallic behavior and the delocalized character of the electrons (Fig. 1). The metallic nature is also reflected in the ground-state wavefunction of the impurity model, which is primarily a single determinant, as seen from the natural orbital occupancies (Table II) and from the impurity wavefunction determinant analysis (Table I). Compared to the restricted HF spectral function, the correlated DMFT spectral function in Fig. 1 displays

TABLE I. Total weight of CI coefficients c_i^2 of different classes of determinants [Hartree–Fock (HF), singly-excited (S), doubly-excited (D)] in the ground-state wavefunction of the impurity model as a function of lattice constant a_0.

excitation level	$a_0 = 1.4$	$a_0 = 2.25$	$a_0 = 2.5$	$a_0 = 6.0$
HF	0.880	0.755	0.676	0.034
S	0.040	0.014	0.087	0.941
D	0.000	0.000	0.098	0.000
number of dets with $c_i^2 > 0.01$	5	8	6	5
$\sum_{c_i^2>0.01} c_i^2$	0.920	0.769	0.861	0.975

additional features at large frequencies and is broader, but the spectra are similar as expected in the weakly correlated regime.

- *Intermediate* regime. At intermediate lattice constants (e.g., 2.25 and 2.5 Å) the spectral function develops a three peak structure with features of both the metallic and insulating regime (Fig. 1). In early DMFT, work on the Hubbard model the central peak was a correlated feature of the spectrum not predicted in mean-field theories.[10,14,40] The two outer peaks are shifted from the ionization potential and electron affinity of the atom. Analysing the impurity wavefunction, we find that at both 2.25 and 2.5 Å lattice constants, the wavefunction has multideterminantal character with significant mixing of open-shell singlets and doubly excited determinants into the ground-state (see Tables I and II).
- *Mott insulator* regime. This occurs at large lattice constants when the hydrogen atoms assume distinct atomic character. This is illustrated by calculations at lattice constant 6.0 Å. (In this limit, the DMFT approximation of a local self-energy becomes exact). The spectral function (Fig. 1) displays an insulating gap and peaks centered at the electron affinity and ionization potential of the hydrogen atom. The impurity wavefunction is a mixture of open-shell singlets (see Table I). We find that the singly occupied impurity natural orbitals (Table II) are respectively localized on the impurity and the bath, thus we characterize the impurity ground-state as an impurity-bath singlet. (Note that the RHF spectral function stays metallic. An unrestricted mean-field calculation would yield two peaks similar to the DMFT spectral function, but at the expense of breaking spin symmetry).

TABLE II. Impurity model natural orbital occupancies for cubic hydrogen (nine bath orbitals) as a function of lattice constant a_0.

	level	1–3	4	5	6	7	8–10
$a_0 = 1.4$	**FCI**	2.000	1.999	1.905	0.095	0.001	0.000
	CISD	2.000	1.999	1.905	0.095	0.001	0.000
$a_0 = 2.25$	**FCI**	2.000	1.998	1.718	0.282	0.002	0.000
	CISD	2.000	1.999	1.720	0.280	0.001	0.000
$a_0 = 2.5$	**FCI**	2.000	1.999	1.528	0.472	0.001	0.000
	CISD	2.000	1.999	1.531	0.469	0.001	0.000
$a_0 = 6.0$	**FCI**	2.000	2.000	1.000	1.000	0.000	0.000
	CISD	2.000	2.000	1.000	1.000	0.000	0.000

B. A configuration interaction impurity solver

As described in Sec. II C, once the impurity model Hamiltonian has been defined, we can determine the impurity Green's function within a wavefunction formalism. Here we investigate the use of the CI hierarchy to construct impurity solvers. We can also see this as using the DMFT framework to extend configuration interaction to the infinite system. To the best of our knowledge, truncated configuration interaction has not previously been explored in the DMFT literature, although full configuration interaction (exact diagonalization) has been widely used.[11,42] By considering CI at an arbitrary excitation level, we obtain a hierarchy of impurity solvers that can, with increasing effort, be systematically converged to the exact full CI limit, within the given bath parametrization. We have based our implementation on the arbitrary excitation level CI program in DALTON.[37] Our code allows the additional possibility of defining restricted active spaces.[43] However, for the simple cubic hydrogen model, we find that the restricted active space methodology is not necessary. Detailed studies of the active space flexibility of the solver will thus be presented elsewhere.

To carry out CI, we define a starting determinant in a "molecular orbital" basis. Note that this is quite different from how exact diagonalization is used in DMFT, where the one-particle basis is chosen to simply be the site basis (atomic orbital basis) of the impurity and the bath. Of course, the result of exact diagonalization is independent of the choice of one-particle basis, and in model problems (such as the Hubbard model), the Hamiltonian has a particularly simple local form in the site basis of the impurity and bath. However, for truncated configuration interaction the choice of starting orbital basis is of course much more important. Here, we take the molecular orbitals to be the eigenfunctions of the Fock operator of the impurity and bath Hamiltonian $H_{imp+bath}$, Eq. (23) [this is obtained by replacing the impurity part of the Hamiltonian by the impurity Fock operator $\mathbf{f}$ appearing in Eq. (30)]. From the lowest energy orbitals we then populate a ground-state determinant and define the set of singles, doubles, and higher excited determinant spaces as in a conventional CI approximation. We calculate the ground-state impurity wavefunction within the given CI space, generating a CI vector ψ and a ground-state energy $E_{imp+bath}$. We then evaluate the Green's function (28) by solving the two intermediate linear equations for $\bar{\mathbf{X}}_i$, and $\mathbf{X}_j$

$$[(\omega + \mu + E_{imp+bath})\mathbf{1} - \mathbf{H}_{imp+bath})]\bar{\mathbf{X}}_i(\omega) = \bar{\mathbf{B}}_i,$$
$$\bar{\mathbf{B}}_i = \bar{\mathbf{C}}_i\psi, \tag{33}$$

$$[(\omega + \mu - E_{imp+bath})\mathbf{1} + \mathbf{H}_{imp+bath})]\mathbf{X}_j(\omega) = \mathbf{B}_j,$$
$$\mathbf{B}_j = \mathbf{C}_j\psi \tag{34}$$

where $\mathbf{C}_i$, $\bar{\mathbf{C}}_i$, $\mathbf{H}_{imp+bath}$ are representations of the impurity orbital creation, annihilation operators and impurity and bath Hamiltonian operator in the truncated CI space. (Note, for the

$N+1$ and $N-1$ particle spaces accessed by the creation and annihilation operators, we consider the space of all determinants that are connected to the N particle truncated CI space for the ground-state calculation). ω can be either purely imaginary (as used in the DMFT self-consistency cycle) or it can be real, with a small imaginary broadening $i\eta$, when calculating the spectral function. The Green's function matrix element is then obtained via

$$G_{ij} = \mathbf{B}_i \bar{\mathbf{X}}_j + \bar{\mathbf{B}}_j \mathbf{X}_i \tag{35}$$

The solution of the linear equations (35) can be achieved via a variety of iterative algorithms. Our implementation follows the algorithm for CI response properties described in Ref. 44 adapted to truncated CI spaces.

Our calculations have demonstrated that in the molecular orbital basis the modest variant of truncated configuration interaction, namely CISD, where the Hilbert space is truncated to contain only singly and doubly excited determinants, was completely sufficient to illustrate all the regimes of the hydrogen solid. In Fig. 1 and Table II, we show the CISD and FCI local spectral function and impurity natural orbital occupations in the three electronic regimes of cubic hydrogen. In the metallic regime, the CISD spectral function is completely indistinguishable from the FCI spectral function, and the same is true for the impurity orbital natural occupation numbers. In the intermediate regime, for the lattice spacings 2.25 and 2.5 Å we expect correlation effects to be stronger. However, the impurity natural orbital occupations show that there are only two natural orbitals with significant partial occupancy, and thus CISD is a very good approximation to FCI. This is reflected in both the spectral functions in Fig. 1 where CISD and FCI agree very well, as well as in the natural orbital occupation numbers, although CISD is not as close an approximation in this case to FCI as it is in the metallic regime. Finally, in the Mott insulator regime, the analysis of the occupation numbers shows again that there are only two orbitals with significant partial occupancies and the FCI and CISD spectral functions and impurity natural occupation numbers are again indistinguishable.

The near-exactness of the CISD level of impurity solver is a feature of the simplicity of the cubic hydrogen model system but also reflects the compactness of the CI expansion

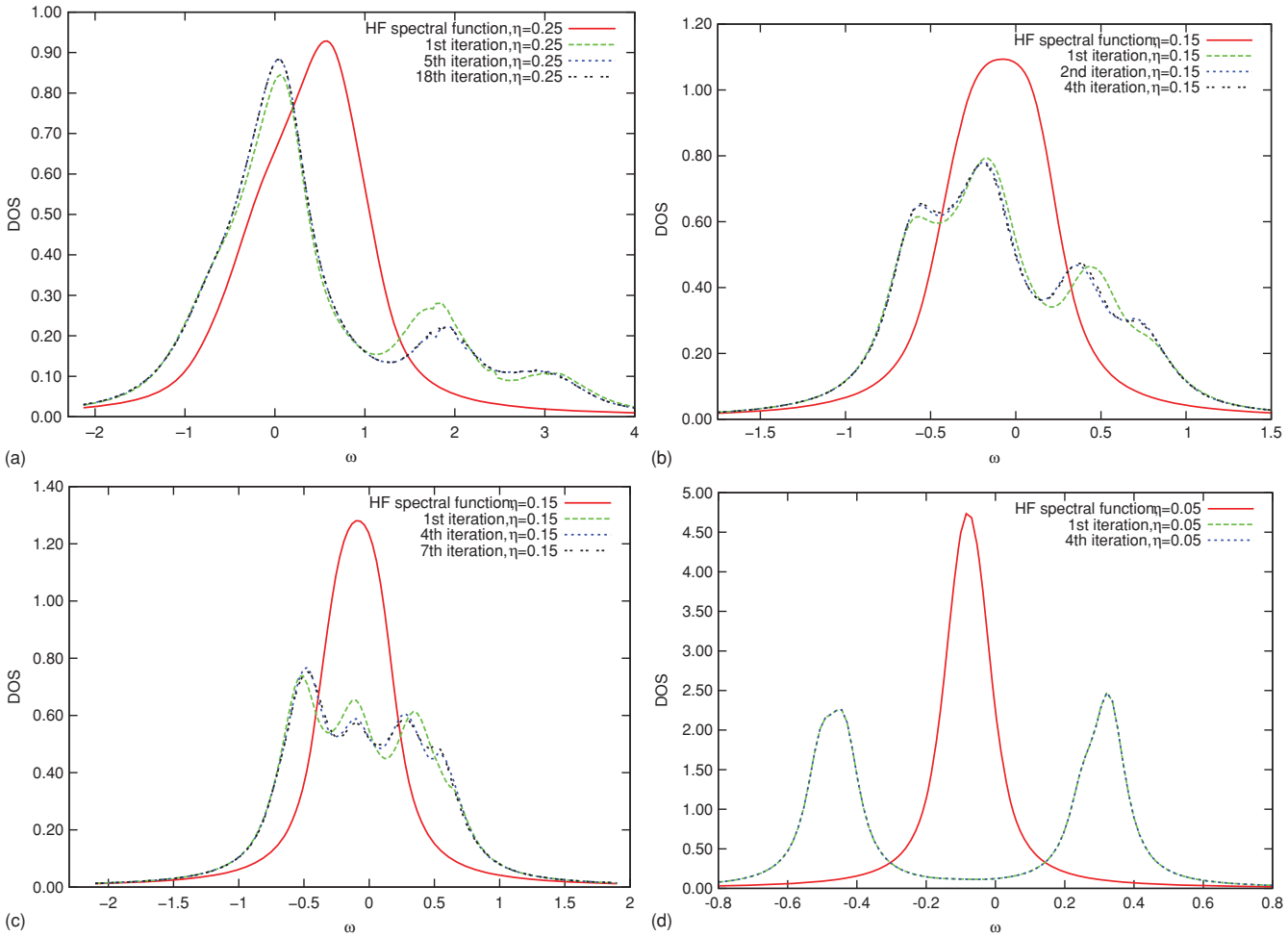

FIG. 2. Spectral function (density of states) obtained with CISD as a solver during the iterations of the self-consistency cycle for cubic hydrogen, at various lattice constants.
(A) $a_0 = 1.40$ Å, 9 bath orbitals, 300 frequency points. **(B)** $a_0 = 2.25$ Å, 9 bath orbitals, 300 frequency points.
(C) $a_0 = 2.50$ Å, 9 bath orbitals, 300 frequency points. **(D)** $a_0 = 6.00$ Å, 9 bath orbitals, 300 frequency points.

when one is using an appropriate one-particle starting basis, in this case the molecular orbital basis rather than the site basis. We expect that more complex solids will pose greater challenges and require higher levels of excitation in the configuration interaction solver, and these issues will be examined elsewhere. Nonetheless, the good performance of the single and doubles level truncation suggests that it will be promising to explore systematic wavefunction hierarchies in more complex problems, which may be infeasible in the exact diagonalization approach.

C. DMFT numerics: self-consistency

As discussed in our overview of DMFT and our specification of our implementation in Sec. III, the impurity model particle number $N_{imp+bath}$, chemical potential μ, and hybridization $\mathbf{\Delta}(\omega)$ and self-energy $\mathbf{\Sigma}(\omega)$ must all be determined self-consistently. The determination of the optimal impurity model particle number and chemical potential are discrete and continuous searches over single variables which are essentially robust. In contrast, the self-consistency condition for $\mathbf{\Delta}(\omega)$ and $\mathbf{\Sigma}(\omega)$ are multidimensional equations. Here we examine the convergence of the self-consistency cycle for the self-energy $\mathbf{\Sigma}(\omega)$ in the loop given by steps 3–6 in algorithm 2.

In Fig. 2, we examine the spectral functions obtained at the CISD level in the three electronic regimes of cubic hydrogen as a function of the number of iterations of the self-consistency cycle. Generally, we find that convergence is very rapid. In the case of the metallic regime, the spectral function appears to converge after five iterations. In the intermediate regime, for lattice constant $a_0 = 2.25$ Å the spectral function also converges after 2 iterations. At the slightly larger lattice constant $a_0 = 2.5$ Å, convergence is a little slower and the spectral function requires four iterations to converge. Finally, as we enter the Mott insulating regime, convergence is once again rapid and the spectral function converges after two iterations.

The same convergence behavior is observed in the electronic structure of the impurity problem. In Table III, we show the natural orbital occupation numbers of the impurity problem corresponding to $a_0 = 2.5$ Å. These numbers were obtained using the CISD solver. (Additional tables corresponding to the other lattice constants are given in the supplementary material[45]). We see that convergence in the 2nd decimal place is reached after five iterations.

Overall, we find that at least for the spectral functions of the cubic hydrogen model, only a few iterations of self-consistency are already sufficient. For quantitative properties, such as an evaluation of the total energy with chemical accuracy, we expect, however, to need a tighter convergence.

TABLE III. Natural orbital occupancies obtained with CISD solver during the iterations of self-consistent cycle for cubic hydrogen, $a_0 = 2.5$ Å, 9 bath orbitals, for exact parameters used to converge self-consistency see supplementary material.

iter/orb no.	1–3	4	5	6	7	8–10
1	2.000	1.999	1.720	0.280	0.001	0.000
2	2.000	1.998	1.583	0.417	0.002	0.000
3	2.000	1.999	1.556	0.444	0.001	0.000
4	2.000	1.999	1.543	0.457	0.001	0.000
5	2.000	1.999	1.537	0.463	0.001	0.000
6	2.000	1.999	1.533	0.467	0.001	0.000
7	2.000	1.999	1.531	0.469	0.001	0.000

D. DMFT numerics: convergence with bath size

As discussed in Sec. II C, when dealing with an explicit bath the hybridization $\mathbf{\Delta}(\omega)$ is parametrized by a finite bath, and all quantities must then be converged with respect to the number of bath orbitals. There are two aspects of bath convergence to explore. How difficult is the numerical problem of fitting the hybridization to the bath couplings ϵ_p and V_{pi}? How rapidly do the relevant correlated quantities (such as the DMFT spectral functions) converge with bath size? In the latter case, the ability of the truncated configuration interaction solver (here CISD) introduced in Sec. IV B to access larger bath sizes than available to exact diagonalization, provides a new capability to examine bath convergence.

We first discuss the numerical fitting and quality of representation of the hybridization $\mathbf{\Delta}(\omega)$ as a function of the number of bath orbitals with couplings ϵ_p and V_{pi}. We determine the bath parameters ϵ_p and V_{pi} by fitting $\mathbf{\Delta}(\omega)$ to the form (24). In principle, one could carry out the fit using any set of frequencies, but following standard practice, we fit along the imaginary frequency axis, where the hybridization is a smooth function, and use an equally spaced set of frequencies ω_n (Matsubara frequencies)

$$\omega_n = \frac{(2n+1)\pi}{\beta}, \; n = 0, 1, 2 \ldots \tag{36}$$

where β, the inverse temperature, determines the spacing. The choice of β is somewhat arbitrary, but to reproduce spectral functions over a given range of frequencies, we find that it is reasonable to take β to correspond to a similar range of frequencies on the imaginary axis.

Fitting to Eq. (24) is a highly nonlinear fit. We find that the final fit quality depends strongly on the initial choice of the parameters. We have established an initialization procedure to obtain a reasonable set of starting ϵ_p and V_{pi}, described in the appendix. From this initial set, we use a Levenberg–Marquadt algorithm to minimize the metric $\sum_{nij} |\Delta_{ij}(\omega_n) - \Delta_{ij}^{fit}(\omega_n)|$ to refine the bath parameters. As described in Sec. II C, the nonorthogonal orbital corrections for the impurity overlap and Hamiltonian (26), (27) are essential for obtaining a reasonable fit when the underlying crystal basis is nonorthogonal. However, we find also that if we artificially set the overlap matrix $\mathbf{S}(\mathbf{k})$ to the unit matrix, and proceed to fit the hybridization functions obtained in this way, considerably better fits are easily obtained. This suggests that it will be more efficient in the future to work within a local orthogonal basis for the crystal, rather than the Gaussian basis currently used.

We show the results of the fitting procedure for the real and imaginary parts of the Hartree–Fock hybridization (defined in Sec. III) in the metallic regime in Fig. 3 and Fig. 4. Similar studies of illustrating difference

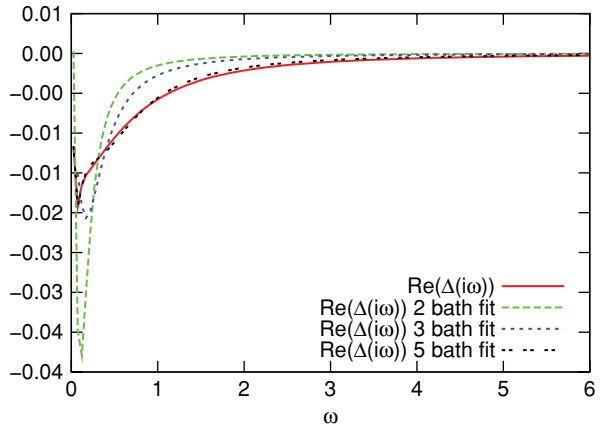

FIG. 3. Fitting accuracy for the real part of the hybridization $Re(\mathbf{\Delta}(i\omega))$ for various numbers of bath orbitals. The number of frequencies employed was 128 and $\beta = 128$.

between Green's functions obtained for different number of bath orbitals can be found in Appendix C of Ref. 11 or for cluster DMFT in Ref. 46. It is evident that the fit becomes better as we increase the number of bath orbitals, and indeed with five bath orbitals the fits appear exact to the eye. However, the quality of the fit along the imaginary axis does not necessarily guarantee the same quality of reproduction of properties along the real axis. In Fig. 5, we show the convergence of the accuracy of the impurity spectral function, $-\frac{1}{\pi}\Im \mathrm{Tr}\mathbf{G}_{imp}(\omega)$ to the corresponding Hartree–Fock quantity $-\frac{1}{\pi}\Im \mathrm{Tr}\mathbf{g}(\mathbf{R}_0, \omega)$. [Note that this is not the physical local spectral function, which must be defined in a nonorthogonal basis with an additional overlap factor, as in Eq. (14)]. For two bath orbitals, the fit on the imaginary axis is poor and the spectral function on the real axis is poorly represented as well. Once the number of bath orbitals is increased to five orbitals, the error of the fit on the imaginary axis becomes quite small and the spectral function becomes appropriately improved. However, the rate of the improvement of the spectral function with respect to the number of bath orbitals is slower than the improvement of the fit on the imaginary axis, as it is much less smooth. Note that

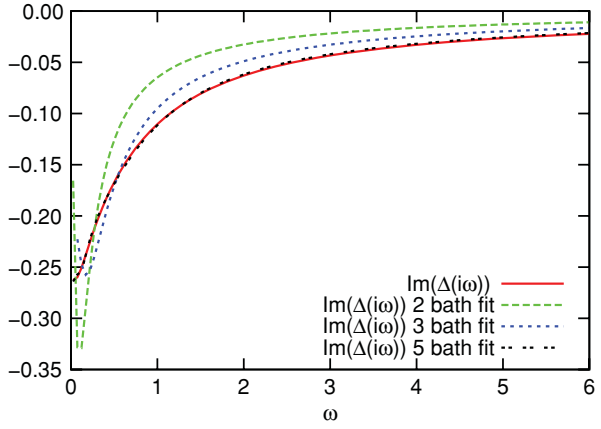

FIG. 4. Fitting accuracy for the imaginary part of the hybridization $Im(\mathbf{\Delta}(i\omega))$ for various numbers of bath orbitals. The number of frequencies employed was 128 and $\beta = 128$.

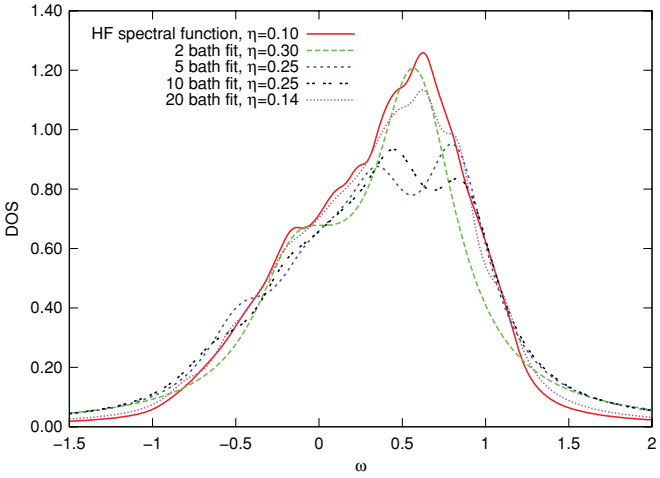

FIG. 5. Fitting accuracy with different number of bath orbitals for the Hartree–Fock impurity spectral function of cubic hydrogen. The number of frequencies employed was 128 and $\beta = 128$.

for each of the spectral functions in Fig. 5, we have chosen a different broadening parameter η to reflect the changing bath orbital spacing.

We now turn to the convergence of the correlated DMFT quantities as a function of bath size. The need to examine this convergence is an essential feature of working within the discrete bath formulation. In Fig. 6, we present the cubic hydrogen local spectral functions obtained using the CISD method as a solver at lattice constant 2.25 Å using 5, 9, and 19 bath orbitals in the impurity model, the latter bath size being comfortably beyond what can be studied using exact diagonalization. In addition, in Table IV we also present the impurity natural occupation numbers calculated with CISD solver with the different bath sizes as a more quantitative test of the bath size convergence. Similar studies of the convergence of the occupation numbers with respect of to the bath size while using exact diagonalization as a solver can be found in Ref. 46 and 47.

We see that the spectral functions are in fact quite similar between the different bath sizes. Indeed already the very small

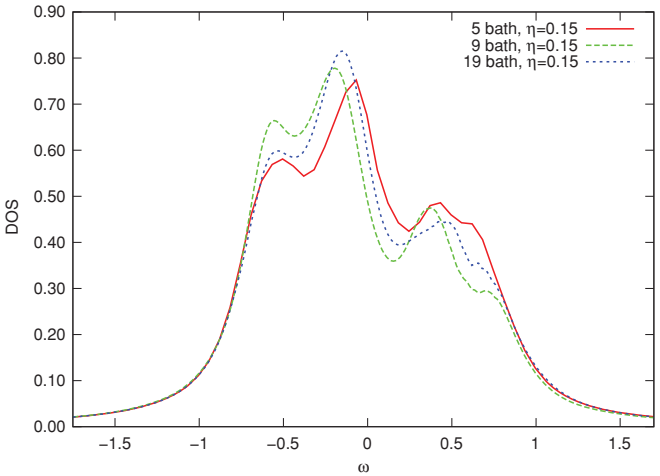

FIG. 6. Spectral function (density of states) obtained with CISD solver for different number of bath orbitals for cubic hydrogen, $a_0 = 2.25$ Å.

TABLE IV. Impurity natural orbital occupancies obtained with CISD solver for cubic hydrogen at lattice constants 2.25 Å, using 5, 9, and 19 bath orbitals.

5 bath	1	2	3	4	5	6
$a_0 = 2.25$	2.000	1.999	1.710	0.290	0.001	0.000
9 bath	1–3	4	5	6	7	8–10
$a_0 = 2.25$	2.000	1.999	1.720	0.280	0.001	0.000
19 bath	1–8	9	10	11	12	13–20
$a_0 = 2.25$	2.000	1.999	1.739	0.261	0.001	0.000

5 bath orbital result is remarkably similar to the 19 bath orbital result. This must be considered a feature of the simplicity of the cubic hydrogen model which has only a single orbital in the unit cell. Examining the impurity model natural occupation numbers we also see that all bath orbital sizes yield very similar natural occupancies with only very small differences. This is promising for future applications as it seems only a relatively small number of bath orbitals is necessary to obtain a converged result.

V. CONCLUSIONS

In this work, we have carried out an initial study of dynamical mean-field theory (DMFT) from a quantum chemical perspective. DMFT provides a powerful framework to extend quantum chemical correlation hierarchies to infinite problems through a self-consistent embedding view of the crystal. The basic approximation is one of a local self-energy, which is a kind of local correlation approximation.

We have explored several ways in which quantum chemical ideas can be combined with the DMFT framework. First, we start with a Hartree–Fock based DMFT Hamiltonian which avoids the double counting problems of the commonly employed DFT-DMFT scheme. Second, we have investigated the truncated configuration interaction (CISD) as an impurity solver. The CI hierarchy avoids the sign problem inherent to Monte Carlo solvers in DMFT, and allows a systematically improvable approach to the exact solution. Conversely, the DMFT framework enables even truncated CI to be extended to the infinite crystal. In the simple but challenging cubic hydrogen model we find that CI at the singles and doubles level already reproduces the structure of the density of states in the various electronic regimes with near perfect accuracy. Finally, we have carried out an investigation of some numerical aspects of the DMFT procedure, including convergence of the self-consistent cycle and convergence of properties with respect to the bath discretization. We find that modest bath sizes, easily accessible to the CI solver, already produce converged results.

These investigations should be viewed as first steps and there are many avenues to develop these ideas. For example, the Hartree–Fock starting point in DMFT treats long-range Coulomb interactions at only the mean-field level, neglecting long-range screening. Quantum chemical perturbation techniques may be useful in treating these additional interactions and may prove complementary to current Green's function treatments of screening.[8,31] Also, there is a wealth of quantum chemical wavefunction approximations that could be combined with the DMFT framework, the most obvious example being coupled cluster theory, which should prove advantageous over configuration interaction as the number of impurity orbitals increases.

Additionally, the main ideas in this work, in particular, the use of quantum chemical Hamiltonians and solvers, are not limited to the single orbital DMFT that we have used to study cubic hydrogen. Their combination with multiorbital and cluster versions of DMFT[17,48–50] should be investigated. Finally, the possibility of using DMFT in finite and inhomogeneous systems,[51] either within the standard DMFT formalism[52,53] or through a true finite DMFT formalism,[21] or the use of DMFT ideas with quantum variables other than the Green's function are further intriguing possibilities for the future.

ACKNOWLEDGMENTS

This work was supported by the Department of Energy (DOE), Office of Science. We acknowledge useful conversations with A. J. Millis, C. A. Marianetti, D. R. Reichman, E. Gull, and G. Kotliar.

APPENDIX: GUESS FOR BATH FITTING

To generate some initial guess bath parameters ϵ_p and V_{pi} for the bath fitting, we follow the procedure below. Let us specialize to the case of a single impurity orbital where we can drop the i index. Then the bath parametrization (24) becomes

$$\Delta(\omega_n) = \sum_p \frac{V_p^2}{\omega_n - \epsilon_p}, \tag{A1}$$

where we have assumed V_p is real. Viewing $1/(\omega_n - \epsilon_p)$ as the elements of a matrix $M_{np} = 1/(\omega_n - \epsilon_p)$, the above becomes the matrix equation

$$\Delta_n = \sum_p M_{np} W_p, \tag{A2}$$

where $\Delta_n = \Delta(\omega_n)$ and $W_p = V_p^2$. We can invert this equation to obtain the couplings

$$W_p = \sum_n M_{pn}^{-1} \Delta_n, \tag{A3}$$

where we understand $\mathbf{M}^{-1}$ to mean the generalized inverse in the singular value decomposition sense. There are now only two remaining issues. First, we have to choose a set of ϵ_p to define the matrix $\mathbf{M}$. Second, given arbitrary $\mathbf{\Delta}_n$, W_p is not necessarily positive definite (and thus does not necessarily yield real couplings V_p). We find the latter to be a problem particularly when the overlap matrix (due to nonorthogonality) is significantly different from unity, which further suggests (as discussed in Sec. IV D) that it will be advantageous to work in an orthogonal basis in the future.

In the first case, we take roots of the Legendre polynomial of order $P/2$ where P is the number of bath levels we wish to fit and map them respectively from the $[-1, 1]$ interval

(associated with the Legendre roots) to $[0, \infty]$ and $[-\infty, 0]$ using the transformation $1 - x/(\lambda(1 + x))$, where λ is a scaling factor that is optimized to produce the best fit. In the second case, we simply take $V_p = \Re(W_p^{-1/2})$.

[1] T. Helgaker, P. Jorgensen, and J. Olsen, *Molecular Electronic-Structure Theory* (Wiley, New York, 2000).
[2] P. Y. Ayala and G. E. Scuseria, J. Chem. Phys. **110**, 3660 (1999).
[3] B. Doser, D. S. Lambrecht, J. Kussmann, and C. Ochsenfeld, J. Chem. Phys. **130**, 064107 (2009).
[4] H.-J. Werner, F. R. Manby, and P. J. Knowles, J. Chem. Phys. **118**, 8149 (2003).
[5] Y. Yang, Y. Kurashige, F. R. Manby, and G. K. Chan, J. Chem. Phys. **134**, 044123 (2011).
[6] S. Hirata, Phys. Chem. Chem. Phys. **11**, 8397 (2009).
[7] A. F. Izmaylov and G. E. Scuseria, Phys. Chem. Chem. Phys. **10**, 3421 (2008).
[8] C. Pisani, M. Busso, G. Capecchi, S. Casassa, R. Dovesi, L. Maschio, C. Zicovich-Wilson, and M. Schütz, J. Chem. Phys. **122**, 094113 (2005).
[9] A. Georges, AIP Conf. Proc. **715**, 3 (2004).
[10] A. Georges and G. Kotliar, Phys. Rev. B **45**, 6479 (1992).
[11] A. Georges, G. Kotliar, W. Krauth, and M. J. Rozenberg, Rev. Mod. Phys. **68**, 13 (1996).
[12] K. Held, Adv. Phys. **56**, 829 (2007).
[13] K. Held, I. A. Nekrasov, G. Keller, V. Eyert, N. Bluemer, A. K. McMahan, R. T. Scalettar, T. Pruschke, V. I. Anisimov, and D. Vollhardt, Phys. Status Solidi **243**, 2599 (2006).
[14] M. Jarrell, Phys. Rev. Lett. **69**, 168 (1992).
[15] G. Kotliar, S. Y. Savrasov, K. Haule, V. S. Oudovenko, O. Parcollet, and C. A. Marianetti, Rev. Mod. Phys. **78**, 865 (2006).
[16] W. Metzner and D. Vollhardt, Phys. Rev. Lett. **62**, 324 (1989).
[17] T. Maier, M. Jarrell, T. Pruschke, and M. H. Hettler, Rev. Mod. Phys. **77**, 1027 (2005).
[18] R. A. Friesner and V. Guallar, Ann. Rev. Phys. Chem. **56**, 389 (2005).
[19] P. Huang and E. A. Carter, J. Chem. Phys. **125**, 084102 (2006).
[20] T. Wesolowski and A. Warshel, J. Chem. Phys. **98**, 5183 (1994).
[21] N. Lin, C. A. Marianetti, A. J. Millis, and D. R. Reichman, arXiv:1010.3180v1 (2010).
[22] A. L. Fetter and J. D. Walecka, *Quantum Theory of Many–Particle Systems* (McGraw-Hill, New York, 1971).
[23] J. E. Hirsch and R. M. Fye, Phys. Rev. Lett. **56**, 2521 (1986).
[24] E. Gull, P. Werner, O. Parcollet, and M. Troyer, Europhys. Lett. **82**, 57003 (2008).
[25] A. N. Rubtsov and A. I. Lichtenstein, JETP Lett. **80**, 61 (2004).
[26] A. N. Rubtsov, V. V. Savkin, and A. I. Lichtenstein, Phys. Rev. B **72**, 035122 (2005).
[27] P. Werner, A. Comanac, L. de' Medici, M. Troyer, and A. J. Millis, Phys. Rev. Lett. **97**, 076405 (2006).
[28] E. Gull, J. A. Millis, A. I. Lichtenstein, A. N. Rubtsov, M. Troyer, and P. Werner, arXiv:1012.4474v1 (2010).
[29] M. Caffarel and W. Krauth, Phys. Rev. Lett. **72**, 1545 (1994).
[30] V. I. Anisimov, F. Aryasetiawan, and A. I. Lichtenstein, J. Phys.: Condens. Matter **9**, 767 (1997).
[31] F. Aryasetiawan, S. Biermann, and A. Georges, in *Correlation Spectroscopy of Surfaces, Thin Films, and Nanostructures*, edited by J. Berakdar and J. Kirschner (Wiley-VCH Verlag GmbH & Co. KGaA, Weinheim, FRG, 2005).
[32] P. H. Dederichs, S. Blügel, R. Zeller, and H. Akai, Phys. Rev. Lett. **53**, 2512 (1984).
[33] H. Meider and M. Springborg, J. Phys.: Condens. Matter **10**, 6953 (1998).
[34] M. Karolak, G. Ulm, T. Wehling, V. Mazurenko, A. Poteryaev, and A. Lichtenstein, J. Electron Spectrosc. Relat. Phenom. **181**, 11 (2010); in *Proceedings of International Workshop on Strong Correlations and Angle-Resolved Photoemission Spectroscopy*, Zurich, Switzerland, 19–24 July, 2009.
[35] R. Pollet, A. Savin, T. Leininger, and H. Stoll, J. Chem. Phys. **116**, 1250 (2002).
[36] R. Dovesi, V. R. Saunders, R. Roetti, *et al.*, CRYSTAL06 *user's manual*, University of Torino, Torino, 2006.
[37] DALTON, a molecular electronic structure program, release 2.0 (2005), see http://www.kjemi.uio.no/software/dalton/dalton.html.
[38] J. Hachmann, W. Cardoen, and G. K.-. L. Chan, J. Chem. Phys. **125**, 144101 (2006).
[39] T. Tsuchimochi and G. E. Scuseria, J. Chem. Phys. **131**, 121102 (2009).
[40] G. Kotliar and D. Vollhardt, Phys. Today **57**, (53) (2004).
[41] X. Y. Zhang, M. J. Rozenberg, and G. Kotliar, Phys. Rev. Lett. **70**, 1666 (1993).
[42] M. Capone, L. de' Medici, and A. Georges, Phys. Rev. B **76**, 245116 (2007).
[43] H. J.A. Jensen, H. Ågren, and J. Olsen, in "Sirius: a general-purpose direct second-order MCSCF program," *Modern Techniques in Computational Chemistry*, edited by E. Clementi (ESCOM, Leiden, The Netherlands, 1991).
[44] H. Koch and R. Harrison, J. Chem. Phys. **95**, 7479 (1991).
[45] See supplementary material at http://dx.doi.org/10.1063/1.3556707 for additonal tables with occupation numbers for different lattice constants; exact parameters used to converge the size consistency.
[46] E. Koch, G. Sangiovanni, and O. Gunnarsson, Phys. Rev. B **78**, 115102 (2008).
[47] M. Capone, M. Civelli, S. S. Kancharla, C. Castellani, and G. Kotliar, Phys. Rev. B **69**, 195105 (2004).
[48] M. H. Hettler, M. Mukherjee, M. Jarrell, and H. R. Krishnamurthy, Phys. Rev. B **61**, 12739 (2000).
[49] M. H. Hettler, A. N. Tahvildar-Zadeh, M. Jarrell, T. Pruschke, and H. R. Krishnamurthy, Phys. Rev. B **58**, R7475 (1998).
[50] G. Kotliar, S. Y. Savrasov, G. Pálsson, and G. Biroli, Phys. Rev. Lett. **87**, 186401 (2001).
[51] V. Dobrosavljević and G. Kotliar, Phys. Rev. Lett. **78**, 3943 (1997).
[52] D. Jacob, K. Haule, and G. Kotliar, Phys. Rev. Lett. **103**, 016803 (2009).
[53] D. Jacob, K. Haule, and G. Kotliar, Phys. Rev. B **82**, 195115 (2010).